

See discussions, stats, and author profiles for this publication at: <https://www.researchgate.net/publication/26697937>

# New Insights into the Activation of Escherichia coli Tyrosine Kinase Revealed by Molecular Dynamics Simulation and Biochemical Analysis

ARTICLE in BIOCHEMISTRY · SEPTEMBER 2009

Impact Factor: 3.02 · DOI: 10.1021/bi900811p · Source: PubMed

---

CITATIONS

8

READS

41

## 5 AUTHORS, INCLUDING:



Tian Lu

Beijing Kein Research Center for Natural Sci...

31 PUBLICATIONS 873 CITATIONS

[SEE PROFILE](#)



Hongwei Tan

Beijing Normal University

42 PUBLICATIONS 456 CITATIONS

[SEE PROFILE](#)



Guangju Chen

Beijing Normal University

85 PUBLICATIONS 1,047 CITATIONS

[SEE PROFILE](#)

## New Insights into the Activation of *Escherichia coli* Tyrosine Kinase Revealed by Molecular Dynamics Simulation and Biochemical Analysis<sup>†</sup>

Tian Lu,<sup>‡</sup> Hongwei Tan,<sup>\*,‡</sup> Daniel Lee,<sup>§</sup> Guangju Chen,<sup>‡</sup> and Zongchao Jia<sup>\*,§</sup>

<sup>‡</sup>Department of Chemistry, Beijing Normal University, Beijing 100875, People's Republic of China, and <sup>§</sup>Department of Biochemistry, Queen's University, Kingston, Ontario K7L 3N6, Canada

Received May 11, 2009; Revised Manuscript Received July 23, 2009

**ABSTRACT:** *Escherichia coli* tyrosine kinase (Etk) regulates the export of pathogenic capsular polysaccharide (CPS) by intermolecularly autophosphorylating its C-terminal tyrosine cluster. The kinase Etk, however, needs to be first activated by the intramolecular phosphorylation of a tyrosine residue, Y574, next to the active site. The recently determined structure of Etk shows that dephosphorylated Y574 blocks the active site and prevents substrate access. After phosphorylation, the negatively charged P-Y574 side chain was previously postulated to flip out to associate with a positively charged R614, unblocking the active site. This proposed activation is unique among protein kinases; however, there is no direct structural evidence in support of this hypothesis. In this paper, we carried out molecular dynamics simulation, mutagenesis, and biochemical analysis to study the activation mechanism of Etk. Our simulation results are in excellent agreement with the proposed molecular switch involving P-Y574 and R614 in the activation of Etk. Further, we show that a previously unidentified residue, R572, modulates the rotation of the P-Y574 side chain through electrostatic interaction, slowing down the opening of the active site. Our enzymatic assays demonstrate that the R572A mutant of Etk possesses significantly increased kinase activity, providing direct experimental support for the unique activation mechanism of Etk. In addition, the simulation of the Etk Y574F mutant predicted short periods of unblocked active site by Y574F, in good agreement with the low kinase activity of this mutant. The C-terminal substrate peptide and the nucleotide cofactor were also docked into the active site, and their implications are discussed.

Extracellular and capsular polysaccharides (EPS and CPS, respectively) are secreted by many bacterial strains, such as *Escherichia coli*. The CPSs adhere to the outer membrane to form the capsule to protect the bacteria from the immune system of the host, preserve water, and promote the absorption of metal ions (1). There are four known assemblies for CPS secretion in *E. coli*. Groups 1 and 4 CPSs are secreted via similar pathways involving polymerase Wzy on the inner membrane (2). According to the current model of the Group 1 pathway (Figure 1A), the polymerized polysaccharides are then exported across the outer membrane through a transmembrane channel consisted of eight molecules of Wza (2–4). The function of Group 1 CPS export assembly depends upon a protein tyrosine kinase, Wzc, which has a tyrosine cluster at its C terminus in the cytoplasm (5). Recent research suggested that a medium level of phosphorylation of this C-terminal tyrosine cluster, possibly through cycling between high and low states of phosphorylation, promotes CPS export (6–8). Wzc intermolecularly autophosphorylates this C-terminal tyrosine cluster, which can be dephosphorylated by phosphatase Wzb. In the similar Group 4 pathway, *E. coli* tyrosine kinase (Etk) is the equivalent regulatory kinase of Wzc (9, 10) (Figure 1A). It is still unclear how the kinase regulates

the channel through the level of phosphorylation on the Wzc or Etk C-terminal tyrosine cluster, modulating the export of CPS.

Since the beginning of the research on prokaryote tyrosine phosphorylation in the past decade, *E. coli* tyrosine kinases Wzc and Etk have attracted most of the attention. Wzc and Etk are inner-membrane proteins with two domains, the N-terminal periplasmic domain and the C-terminal cytoplasmic domain (Figure 1B). The cytoplasmic domain, which is sufficient for kinase activity, contains the catalytic motifs of Walker A (GKT/S), Walker A' (DXD), and Walker B (a downstream D following a series of hydrophobic residues). The Walker-A motif is responsible for the binding of ATP; the aspartic residues of Walker-A' and Walker-B motifs are responsible for stabilizing the Mg<sup>2+</sup> and the substrate OH group in the reaction intermediate (11, 12). At the C terminus lies a cluster of several tyrosine residues, which are found in all homologues in Gram-negative and -positive bacteria (13).

The activation of Wzc and Etk follows a two-step mechanism involving both intra- and intermolecular phosphorylation (panels C and D of Figure 1). The kinase first intramolecularly autophosphorylates a conserved upstream tyrosine residue (Y569 in Wzc and Y574 in Etk), drastically increasing its kinase activity (14). Once activated, the kinase further phosphorylates the C-terminal tyrosine cluster through an intermolecular reaction. The molecular mechanism of this two-step activation remained a mystery until the high-resolution structure of the Etk kinase domain became available recently (11) (Figure 1E). On the basis of the structure, as well as the mutational and functional studies, a probable explanation for Etk activation via

<sup>†</sup>This work was funded by the Science Foundation of the National Science Foundation of China, the Major State Basic Research Development Program, and the Canadian Institutes of Health Research. Z.J. is a Canada Research Chair in Structural Biology.

<sup>\*</sup>To whom correspondence should be addressed. Telephone: (+1) 613-5336277. Fax: (+1) 613-5332497. E-mail: hongwei.tan@bnu.edu.cn (H.T.); jia@queensu.ca (Z.J.).

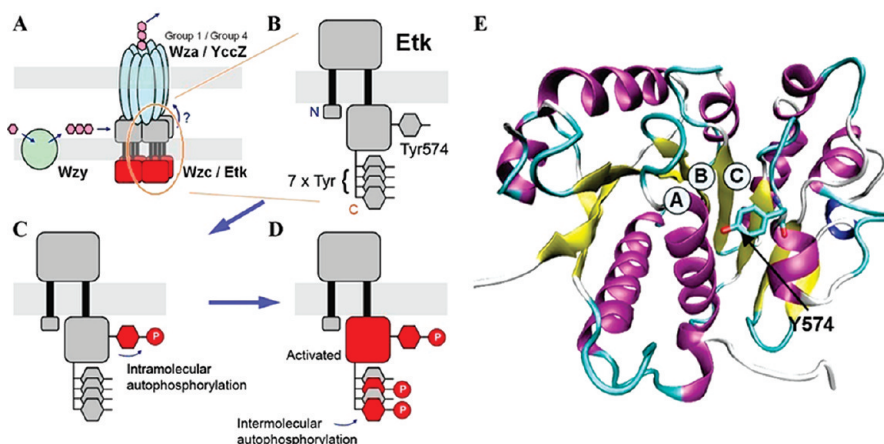


**FIGURE 1:** Schemes of Groups 1 and 4 CPS export and the activation of the protein tyrosine kinase. (A) Probable assembly of the CPS export channel and the tyrosine kinase from a cryo-electron microscopic structure (6). After polymerization by Wzy, polysaccharides are exported across the outer membrane through the channel of an octamer of Wza (Group 1 CPS) or YccZ (Group 4) to form the bacterial capsule. The export is regulated by inner-membrane protein tyrosine kinase Wzc (Group 1 CPS) or Etk (Group 4), although the regulatory mechanism is still unknown. (B) Etk is an inner-membrane protein consisting of a N-terminal periplasmic domain and a C-terminal cytoplasmic domain, which is solely responsible for its kinase activity. Etk contains a C-terminal tyrosine cluster, the phosphorylation level of which is important for CPS export. (C) Activation of Etk first involves the intramolecular autophosphorylation of Tyr574. (D) Subsequently, the C-terminal tyrosine cluster is autophosphorylated intermolecularly. (E) From the structure of Etk, it was proposed that the phosphorylation of Tyr574 induces the side chain to flip away from the active site for substrates entrance (PDB code 3CIO). A, B, and C, respectively, represent the catalytic Walker-A, Walker-B, and Walker-A' motifs.

autophosphorylation of Y574 was proposed (11). In the dephosphorylated state, the side chain of Y574 was shown in the structure to block the active site of the kinase, preventing substrate access to the Walker motifs inside. When phosphorylated, the side chain of phospho-Y574 was hypothesized to flip in the opposite direction, because of the electrostatic attraction, to associate with the side chain of a conserved arginine residue (R614). The flipped P-Y574 side chain no longer obstructs the active site, thus granting substrate access (11). While this postulated activation mechanism was plausible, the “activated” structure showing the association between P-Y574 and R614 has never been obtained despite persistent efforts, probably because of the loss of phospho-tyrosines during its month-long crystallization period (11). The P-Y574-R614 switch, if correct, would mark a unique class of protein tyrosine kinase activation. The single side chain flipping is in good contrast with the eukaryotic protein tyrosine kinases, where a large activation loop undergoes significant conformational change to modulate active-site access (15).

To verify the molecular switch of P-Y574 and study the dynamic process of the proposed flipping of P-Y574, we applied molecular dynamics (MD), quantum chemistry, and molecular docking, along with mutagenesis and biochemical experiments, to examine the conformation and energy change of the active site, particularly P-Y574 and R614. The interaction of the Etk active site with ATP and substrate was also investigated.

## MODELS AND METHODS

**Preparation of the Modeling System.** The kinase domain of *E. coli* tyrosine kinase Etk [PDB code 3CIO (11)] was used as the model for simulation. Etk residues 483–491 and 704–726 were missing in the crystal structure and were omitted in this simulation. Because they are both far away from the active site and Y574, we do not expect them to significantly hinder the validity of the simulations. Three simulations were performed. In the first simulation, we studied the structural change upon the phosphorylation of Y574 by adding a phosphate group to replace

the hydroxyl group in Y574. In the ADP-bound Etk structure, because Y574 and ADP are already interacting, placement of a phosphate in the current position of Y574 would result in a direct steric conflict, causing severe repulsion and skewing subsequent calculation. Hence, we manually rotated the side chain of phosphorylated Y574 away from ADP to relieve the steric clash. The second and third models, Y574F and R572A, were built by simple amino acid substitution. Identical simulations were performed on all three models (P-Y574, Y574F, and R572A).

**MD Simulation.** All MD simulations were performed using the GROMACS (16) package (version 3.3.3) with GROMOS96 force field (17). We employed the periodic boundary in the simulations, where the Etk monomer was immersed in a cubic box with a length of 68.75 Å, a setting that allowed >8 Å in the minimal distance between the protein surface and the box wall. Waters were filled into the space of the box with the extended simple point charge model (SPC/E) (18). The systems were first energy-minimized via the steepest descent approach using a convergence criterion of 1000 kJ mol<sup>-1</sup> nm<sup>-1</sup> with a 0.01 nm step size. Minimization was followed by 30 ps of position-restrained MD simulation. The protein was restrained to its initial position, and the solvent was freely equilibrated. Finally, the product phase was obtained with the whole system simulated for 10 ns without any restraint using an integral time step of 1 fs. To maintain a constant temperature of 310 K in the system, the Berendsen thermostat (19) was applied with a coupling constant  $\lambda = 0.5$  ps; solute and solvent were coupled separately. The pressure was maintained by coupling to a reference pressure of 1 bar with the Parrinello–Rahman barostat, with a time constant of 1.0 ps. The isothermal compressibility was set to  $4.5 \times 10^{-5}$  bar<sup>-1</sup> for water simulations. The cutoff for the short-range electrostatic interactions was set to 15 Å; the long-range interactions were treated with a particle-mesh Ewald (PME) (20) method with a grid width of 1.2 Å and a fourth-order spline interpolation.

The Gaussian03 (21) package was employed to calculate the energy of P-Y574 with quantum chemistry. The structures of

P-Y574 were extracted from the product phase of MD trajectories. The energy calculations within 0–800 ps were carried out using B3LYP (22) density functional method with 6-31G\* basis set (23, 24); energy was calculated every 5 frames. The energy within 0–10 ns were calculated every 25 frames using the same method but with 3-21G\* basis set (25, 26). Atoms close to P-Y574 were treated as background point charges; the charge value was consistent with the corresponding atom type in the force field. The energy presented here excluded the interaction energy between background point charges.

During the MD simulation, the coordinates of the system were saved every 1 ps for subsequent analysis. When root-mean-square deviation (rmsd) was calculated, the whole trajectory was fitted to the first frame using  $C_{\alpha}$  atoms by least-squares method to remove the overall translational and rotational motion. The root-mean-square fluctuations (RMSFs) value of the residue was averaged on the atoms within the residue. The RMSF of the crystal structure was transformed from the *B* factor determined by the experiment with the formula (27)  $\langle \Delta r_i^2 \rangle = 3B_i/(8\pi^2)$ . VMD (28) was used for molecular visualization and structural analysis. Molecular surface graphics was generated using the VMD built-in software MSMS, with a probe radius of 1.4 Å.

**Mutagenesis, Protein Expression, and Purification.** Site-directed mutagenesis of R572A was performed with the Quick-Change site-directed mutagenesis kit (Stratagene) using the primer GATGCCGACTTACCGGCTGGGTATTCGCATA-ACCTTTTACC (underlined codon denotes mutation). The template was the wild-type Etk kinase domain described previously (11). The polymerase chain reaction (PCR) cycles were doubled from the manual protocol and performed in the thermal cycler (Eppendorf). After the success of PCR was confirmed with agarose gel electrophoresis, full-plasmid PCR products were transformed into *E. coli* DH5α cells for plasmid annealing. The resulting pET-His<sub>10</sub>-etk<sub>R572A</sub> construct was transformed into *E. coli* BL21(DE3) cells for protein expression and purification following the identical protocol for wild-type Etk (11).

**Kinase and ATPase Activity Measurement.** We measured the kinase activity of Y572A mutant, along with the wild-type Etk kinase domain as a comparison. A total of 20 μM of the protein samples (in 50 mM Tris at pH 8.5) was incubated with 200 μM of ATP and 200 μM of MgCl<sub>2</sub> at room temperature for 5 min. The ATP solution contained 10 μCi of [ $\gamma$ -<sup>32</sup>P]. The proteins were precipitated from 10 μL of the reaction mixture with 20% tetrachloric acid and washed twice with 500 μL of TCA. The resulting pellet was resuspended with 1 mL of standard Gly SDS buffer and mixed with 5.3 mL of ScintiVerse (Fisher). Scintillation readings were taken from both the protein sample and 10 μL of reaction mixture. Activity for the mutant was determined as the scintillation count ratio of the mutant versus the wild type.

The ATPase activity was measured by detecting the level of inorganic phosphate, which generated a blue color when forming the reduced phospho-molybdate complex. Briefly, protein samples were incubated with 0.2 mg/mL ATP, 4 mM MgCl<sub>2</sub>, 80 mM NaCl, and 25 mM Tris at pH 7.5 and 37 °C for 30 min. Subsequently, 30 μL of the reaction solution was mixed with 10 μL of 10% ascorbic acid and 60 μL of 0.42% ammonium molybdate and incubated at 37 °C for 20 min. The resulting blue color was measured with an Ultrospec spectrometer (Biochrome) for OD<sub>660</sub>.

**Circular Dichroism (CD).** CD was used to detect secondary-structure changes before and after the phosphorylation of Etk and mutant. Etk protein samples were first dialyzed to replace Tris with 50 mM sodium phosphate (pH 8.5) and to remove NaCl, while 1 mM of MgCl<sub>2</sub> was added. The sample was then loaded to a 0.1 mm cylindrical quartz cuvette to be placed in a Chirascan CD spectrometer (Applied Photophysics). Five scans with 1 s data acquisition time were averaged to compute the molar ellipticity, which was plotted against wavelength. For the phosphorylation treatment, the protein sample was incubated in 100 μM ATP for 30 min and the resulting scan was compared to the untreated sample.

## RESULTS AND DISCUSSION

**Overall Simulation and the Structural Stability of the Protein Model.** The side-chain flipping of P-Y574 toward R614, because of the electrostatic attraction between the negative and positive charges, was observed in the simulation. The end-run model of the P-Y574 system is shown in Figure 2B. Figure 3A plots the conformational change (in terms of rmsd) of P-Y574  $C_{\alpha}$  versus time (the phosphorylation event is set at  $t = 0$ ). The rmsd value quickly converged to ~0.15 nm within the first 600 ps and remained stable during the rest of the simulation. From observing the protein model over the simulation, it was obvious that P-Y574 undergoes side-chain flipping starting at 600 ps (a movie is supplied in the Supporting Information), while it was mostly stabilized at the flipped position from 1300 ps onward. Therefore, the 10 ns MD simulation of this study was more than sufficient. The total energy of the system, temperature, mass density, and the volume remained stable throughout the 10 ns simulation period.

The RMSF values of all  $C_{\alpha}$ , which reflect the stability of the individual residues over the simulation, are presented in Figure 3B. The RMSF values derived from the experiment and the simulation correlate well, confirming the validity of the MD results. While the RMSF of residues 452–477 and 498–530 are relatively high, most parts of Etk, especially the residues around the active site (540–580 and 640–650), were stable. Therefore, during and after the flipping of P-Y574, leading to the opening of the active site, Etk maintains its structural rigidity. Our MD results demonstrate that the increase in the kinase activity of Etk is likely not due to the overall structural change, in agreement with previous CD observations (11).

**Two Stages of Conformational Change of P-Y574.** The flipping of P-Y574 took place in two stages in the 10 ns simulation. During the first stage (50–460 ps in the simulation), the phosphate group of P-Y574 turned clockwise to associate with R572 (Figure 2C), an arginine residue close to the active site. During the second stage, which took place between 460 ps and 1.3 ns, the phosphate group of P-Y574 broke free from R572 and rotated clockwise to interact with R614, further away from the active site. P-Y574 then remained associated with R614 for the rest of the simulation. Figure 4A describes the fluctuation of the dihedral P-Y574-N/C<sub>α</sub>/C<sub>β</sub>/C<sub>γ</sub> during the simulation. At the beginning, the average dihedral angle was ~60°. The dihedral angle decreased to ~−90° during 460–1000 ps and maintained at ~−90° to the end of the simulation. In panels B and C of Figure 4, T546-C<sub>α</sub> and P-Y574-C<sub>α</sub> were taken as the reference points to describe the movement of the P-Y574 phosphate group. The angle of T546-C<sub>α</sub>/Y574-N/P-Y574-P (Figure 4B) and the distance between T546-C<sub>α</sub>/P-Y574-P (Figure 4C) both shifted significantly during the first 500 ps, which marked the opening

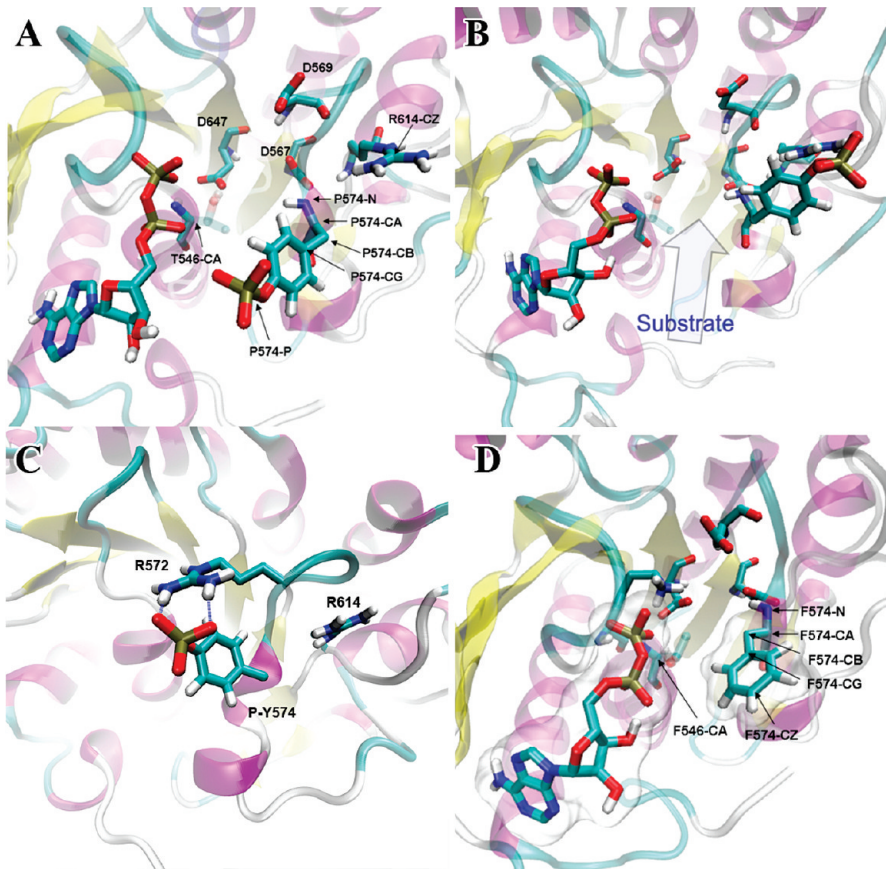


FIGURE 2: Simulation of P-Y574 flipping and the Y574F system. (A) Active site of Etk with phosphorylated Y574. An initial rotation was applied to the side chain of Y574 to avoid the initial steric clash with ADP. Walker-motif residues T546, D567, D569, and D647 are labeled to show the catalytic site. R614 is located on the back side of the P-Y574 side chain. (B) Model at the end of the 10 ns MD simulation. P-Y574 has flipped out to associate with R614. The blue arrow shows the postulated substrate entry into the active site. Y-574 flips to this position at 460 ps. (C) Intermediate state at 423 ps. Y-574 is associated with R572. (D) Final model of the Y574F mutant. The surface of phenylalanine and ADP are shown in transparent gray.

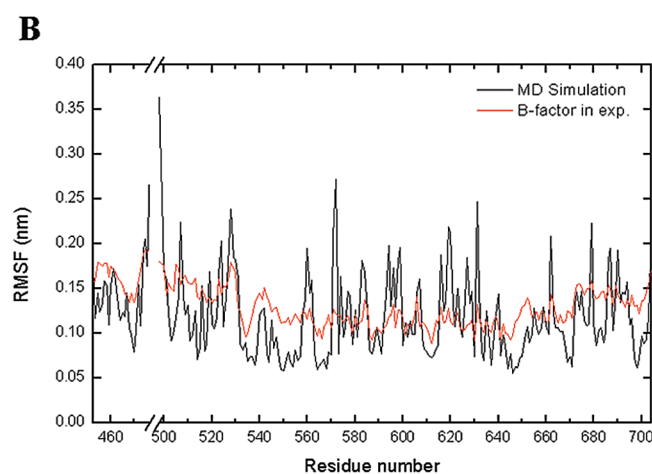
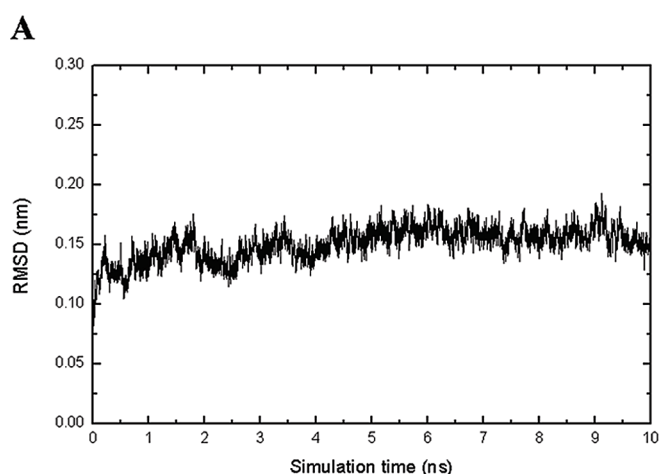


FIGURE 3: Overall stability of Etk in the simulation. (A) rmsd of P-Y574  $C_{\alpha}$  relative to its original position in the crystal structure over the 10 ns simulation. (B) RMSF values of all  $C_{\alpha}$  atoms in the model throughout the simulation. Fluctuation values were obtained by averaging atomic fluctuations over the simulation (black) and computing the value from the *B* factors of the crystal structure (red). Models for residues 478–497 are missing in the crystal structure and, therefore, not shown.

of the active site, while stabilized for the rest of the simulation. In our negative control Y574F system, which lacks the negative charge compared to P-Y574, the above angle and distance remained close to its original value throughout the simulation (panels B and C of Figure 4).

Figure 4D shows the distance between the phosphorus of P-Y574 and  $C_{\beta}$  of R614, which decreased from the initial  $\sim 10.5$

$\text{\AA}$  to  $\sim 4.5 \text{\AA}$  within the first 600 ps, fluctuated back, and again came down to  $\sim 4.5 \text{\AA}$  at 1300 ps. As a result of thermal motion, counterions, and the nearby charged residues, the distance between the two atoms were stabilized at  $\sim 4.5 \text{\AA}$ . The salt bridge between P-Y574 and R614 is particularly important in the stabilization of the flipped state. During 63% of the remaining simulation of 1.5–10 ns, at least one salt bridge is observed

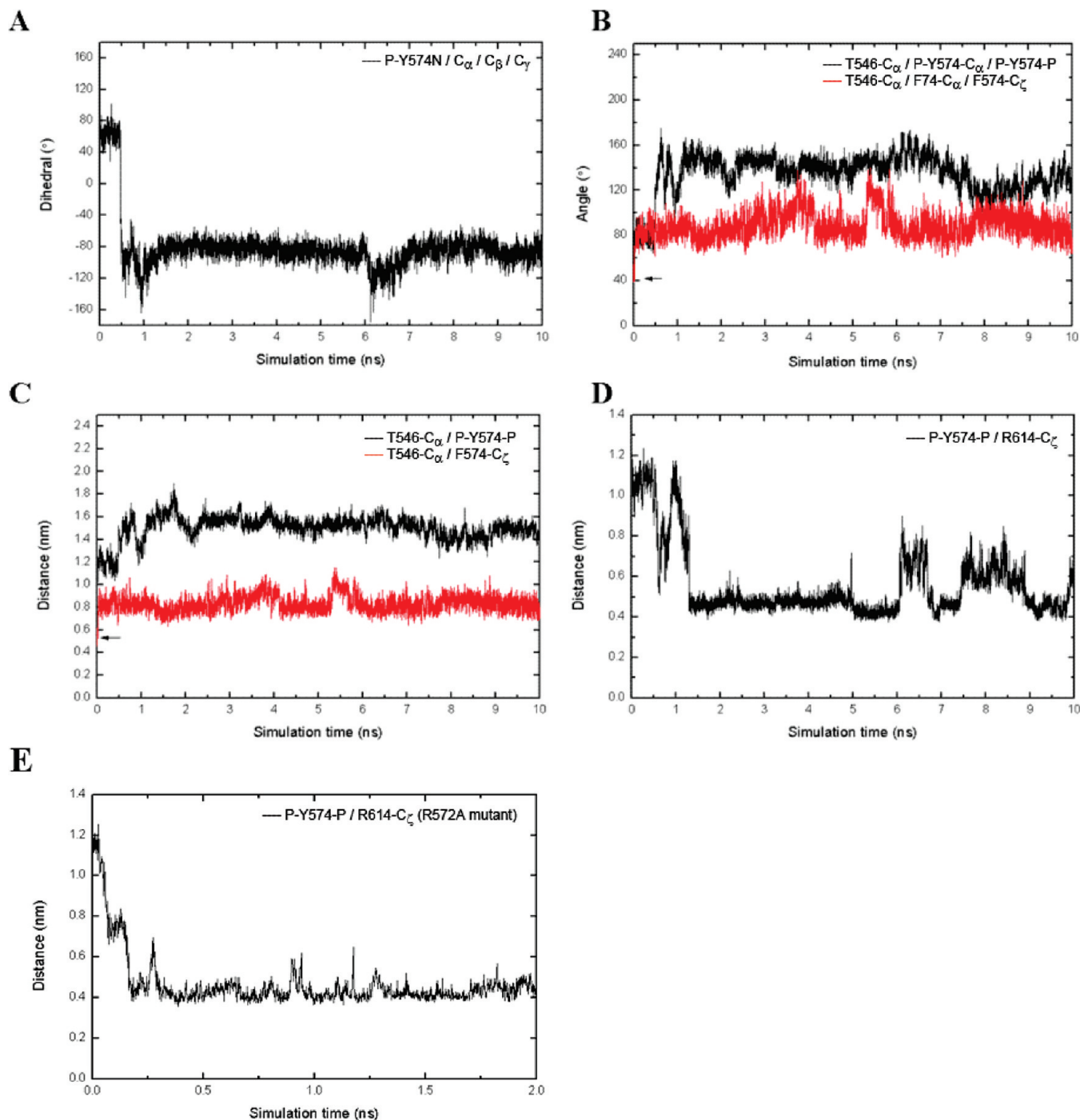


FIGURE 4: Monitoring P-Y574 flipping with angles and distances. (A) Dihedral angle of P-Y574-N/C<sub>α</sub>/C<sub>β</sub>/C<sub>γ</sub> over the 10 ns simulation. (B) Dihedral angles of T546-C<sub>α</sub>/P-Y574-C<sub>α</sub>/P-Y574-P (black) and T546-C<sub>α</sub>/F574-C<sub>α</sub>/F574-C<sub>ζ</sub> (red). (C) Distance between T546-C<sub>α</sub> and P-Y574-P (black) and between T546-C<sub>α</sub> and F574-C<sub>ζ</sub> (red). In B and C, because of the rapid structure movement at the beginning of the simulation, the initial values are marked by black arrows at  $t = 0$ . (D) Distance between P-Y574-P and R614-C<sub>ζ</sub> for the wild-type system (black) for the entire 10 ns simulation and (E) the R572A system for the first 2 ns of the simulation.

between P-Y574 and R614, using the criteria of  $< 30^{\circ}$  and  $< 3.5 \text{ \AA}$  between the interacting atoms. When the criteria are relaxed to  $< 35^{\circ}$  and  $< 4.0 \text{ \AA}$ , the interaction time between P-Y574 and R614 reached 77% in the rest of the simulation. Therefore, the attractive interaction between the P-Y574 and R614 alone is quite intensive and stable.

**R572 Negatively Regulates the Activation of Etk.** While P-Y574 was initially trapped by R572 briefly in the first stage of flipping, the side chain was not far away from the active site and rendered incomplete opening of the active site. Unable to break away from this strong interaction, P-Y574 would “drag” R572

along and continue its movement toward its final “destination”, R614. Therefore, R572 either (1) hinders the activation of Etk by preventing the opening of the active site or (2) promotes the activation of Etk by providing a “flipping intermediate”. To distinguish these two possibilities, we designed the third simulation system involving the R572A mutant. Further, we performed site-directed mutagenesis to produce the actual R572A mutant (Figure 5A) to be tested in the kinase and ATPase activity assays (Figure 5B). We preformed a CD experiment (Figure 5C) to ensure that the mutant is probably folded prior to biochemical characterization and further assess the conformational

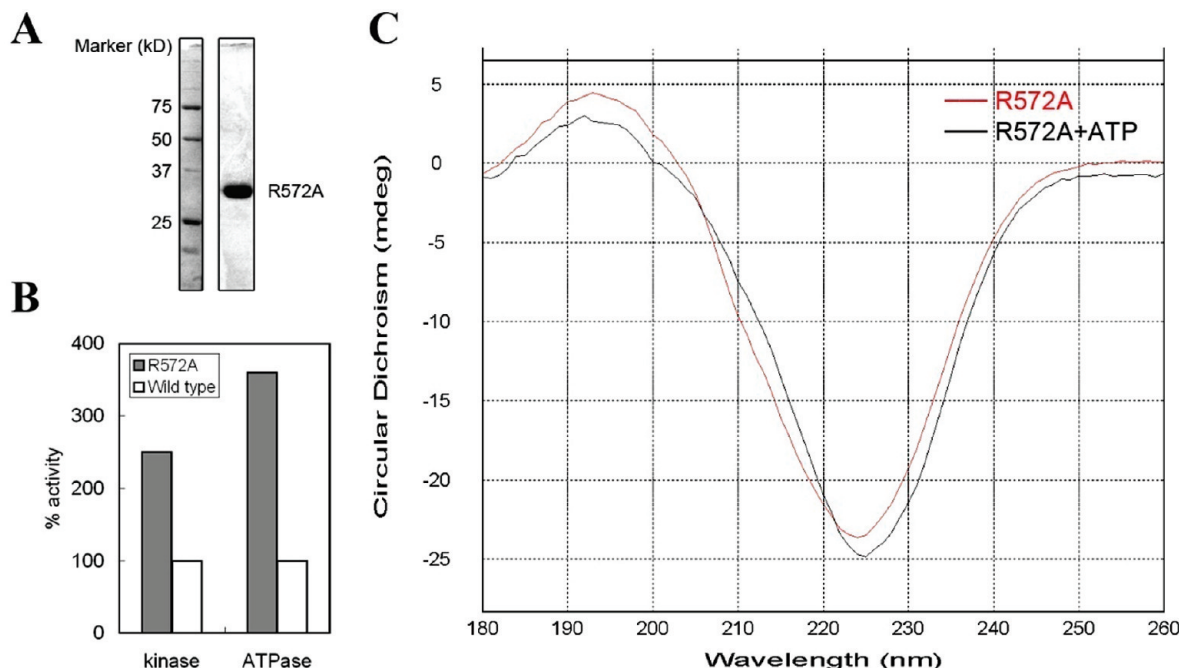


FIGURE 5: Relative activity and CD spectrum of the Etk R572A mutant. (A) Sodium dodecyl sulfate–polyacrylamide gel electrophoresis (SDS–PAGE) gel showing purified Etk R572A. (B) Kinase and ATPase activity of Etk R572A compared to the wild type. (C) CD spectrum of Etk R572A mutant before and after autophosphorylation.

change before and after autophosphorylation of the R572A mutant.

The simulation of the R572A mutant system showed that Y-574 was able to flip and bind to R614 more quickly than the wild type (panels D and E of Figure 4). The flipping process of the R572A system was completed at 250 ps, in contrast to the nearly 1300 ps required for the wild-type system. The overall structural stability for the R572A system was comparable to that of the wild type.

The experimental evidence from the kinase and ATPase activity assays confirmed the simulation result. The R572A mutant, which is properly folded according to the CD spectrum (Figure 5C), possessed 250% of wild-type kinase activity and 360% of wild-type ATPase activity (although the ATPase activities of Etk are very weak in general). The increased kinase activity is therefore due to the removal of the positively charged R572 trap. On the other hand, the reason for the increase in ATPase activity is less obvious. According to our modeling, it is possible that R572 also interacts with the  $\gamma$ -phosphate of ATP. The removal of the R572 positive charge may accelerate the release of the  $\gamma$ -phosphate of ATP in the active site during ATP hydrolysis. Unfortunately, no ATP-bound crystal structure of Etk is currently available. We further measured the CD spectra of the R572A mutant before and after the phosphorylation (Figure 5C). No significant secondary-structural change was detected, meaning that the increase in the R572A mutant activity likely comes from the simple flipping of Y-574 instead of large conformational changes, in accordance with previous observations (11). Interestingly, R572 is a fully conserved residue in Etk homologue Gram-negative bacteria, suggesting that these bacteria prefer weakened protein tyrosine kinase activity, perhaps to optimize the production of the capsule.

**Energy Variation of P-Y574 and the Influence of the Positive Charges on R614.** To understand the flipping of phosphorylated Y574, the energy of P-Y574 in the first 800 ps was calculated. At the very beginning (0–300 ps) of the

simulation, the repulsion in the protein decreased slightly. At 320 ps, the energy level rapidly peaked at 480 ps. At this moment, the flipping of P-Y574, as reflected by the change in the dihedral angle P-Y574-N/C $\alpha$ /C $\beta$ /C $\gamma$ , took place. The peak energy was 92 kcal/mol higher than the average value before flipping. During the flipping process (460–510 ps), with the dihedral angle dropping to  $-120^\circ$  rapidly, the energy also decreased by up to 182 kcal/mol. The energy level then stabilized for the rest of the simulation, with an average value of 49 kcal/mol lower than the initial (unflipped) model. Apparently, the flipped state of P-Y574 is more energetically favorable than the unflipped state. Further, we have calculated the free energy in the flipping process by combining the total electronic energy with calculated entropy, whose values were estimated by performing normal vibrational mode analysis of the structures along the flipping path (Figure 6C). The free energy barrier of the flipping was estimated to be  $\sim$ 100.76 kcal/mol. After the flipping, the total free energy of Etk decreased by  $\sim$ 42.31 kcal/mol, indicating a favorable energy change. These results are consistent with the notion that the P-Y574 conformational change is an energy-favored process, enabling the opening of the active site of Etk.

To assess the importance of R614 and its electrostatic interaction with P-Y574, the positive charge of R614 was artificially removed from the simulation (Figure 6). The resulting average energy level for the uncharged R614 increased by 68 kcal/mol, enough to erase the favored P-Y574 and R614 interaction. The shapes of the energy curves with and without the positive charge on R614 are highly similar (Figure 6A).

Thermal motion and the interaction between the charged atoms and P-Y574 may result in quick fluctuation in conformation and energy during simulation. To fully examine the stability of the new conformation of P-Y574, an average energy analysis covering a longer time would be necessary. Hence, we calculated the energy of P-Y574 over the entire 10 ns simulation period (Figure 6B). It is notable that the energy level after P-Y574 flipping, although occasionally higher than that averaged from

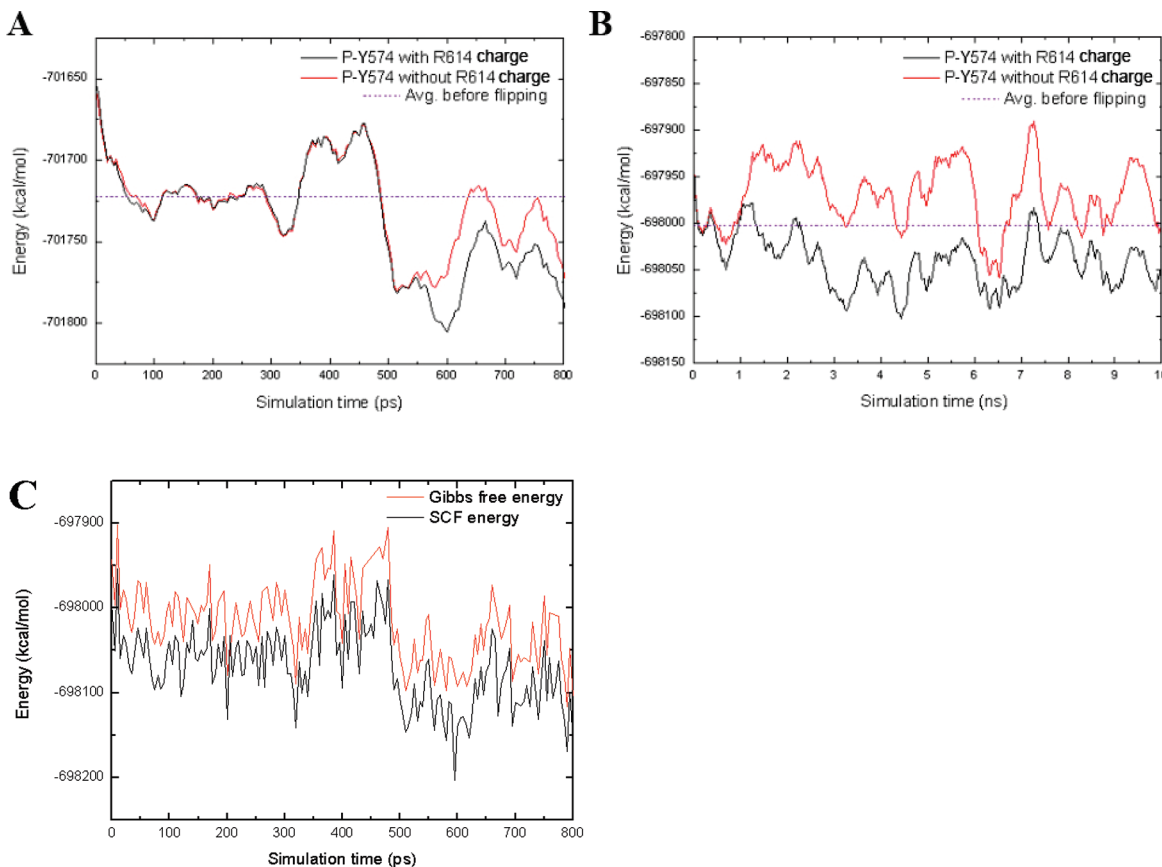


FIGURE 6: Energy change of P-Y574 with and without the positive charge of R614. (A) P-Y574 energy in the presence (black) and absence (red) of the positive charge of R614 in the simulation from 0 to 800 ps and (B) from 0 to 10 ns. The purple dashed line indicates the initial energy of P-Y574 in the unflipped state. (C) Gibbs free energy (red) and the electronic energy (black) of P-Y574 in the simulation from 0 to 800 ps.

the unflipped state, was stabilized at a lowered state, with an average reduction of 43 kcal/mol. When the positive charge on R614 was removed, the energy of the flipped state is higher than the average energy of the unflipped state, with an average increase of 32 kcal/mol. The extent of the energy difference is negatively correlated with the distance between the P-Y574 phosphate group and the R614 guanidine group. Clearly, the flipped conformation of P-Y574 would be unfavorable without the positive charge on R614. Indeed, the kinase activity of Etk mutant R614A was only 14.6% of the wild-type Etk (*II*).

**Conformational Change of the Y574F Mutant.** The Y574F system was intended as a negative control in our simulations. Indeed, there was only a slight change of the monitored dihedral angle and distance; for example, there is a 1.1 Å reduction of the T546-C<sub>α</sub> and F574-C<sub>ξ</sub> distance compared to their regular distance of 6.6 Å during 3.5–4.1 and 5.3–6.0 ns (panels B and C of Figure 4). The conformation of Y574F (Figure 2D) largely remained unchanged throughout the simulation, with an exception of the first 25 ps.

In the crystal structure of the wild-type Etk, a strong hydrogen bond between the Y574 hydroxyl group and the ADP β-phosphate group prevails over the van der Waals repulsion between the two. When Y574 is replaced by a phenylalanine, in the absence of the hydrogen-bonding attraction, the van der Waals repulsion was apparent even in the first 25 ps of the simulation, resulting in a rapid movement of Y574F. The side chain of Y574F rotated considerably in an anti-clockwise manner (Figure 2D). The dihedral angle of F574-N/C<sub>α</sub>/C<sub>β</sub>/C<sub>γ</sub> increased by ~100°, and the angle of T546-C<sub>α</sub>/F574-C<sub>α</sub>/F574-C<sub>ξ</sub> increased

by ~40° (Figure 4B), respectively. The distance between T546-C<sub>α</sub> and F574-C<sub>ξ</sub> also increased by 2.6 Å (Figure 4C).

Judging from the molecular surface shown in Figure 2D, the gap between Y574F and ADP is still too narrow to allow for a tyrosine substrate to approach the catalytic site. However, during 3.5–4.1 and 5.3–6.0 ns, a flipping event similar to that of P-Y574 was observed (Figure 7A). In fact, the peak values of the dihedral angles of F574-N/C<sub>α</sub>/C<sub>β</sub>/C<sub>γ</sub> are similar to those found in the case of P-Y574. It is likely that, during these two short periods, the Y574F side chain is in a similar conformation of the flipped P-Y574, opening the active site for substrate access. It is important to note that the flipped conformation of Y574F is much less stable than that of P-Y574, because the former only accounts for 13% of the entire 10 ns simulation compared to nearly 100% of the latter. Interestingly, the Y574F mutant of Etk was experimentally found to exhibit 12% of the wild-type Etk kinase activity (*II*), an observation that agrees exceptionally well with this simulation. The limited but unmistakable freedom of Y574F, as a result of small-scale molecular movement in solution, provides a reasonable explanation for its weak kinase activity.

Another reason for the low activity of the Y574F mutant may come from its relatively closer position to the active site than P-Y574. Figure 7B shows the comparison of the P-Y574 and Y574F systems in terms of the distance between T546-C<sub>α</sub> and P-Y574-C<sub>α</sub> (F574-C<sub>α</sub>). Because of the electrostatic attraction between R614 and P-Y574, the C<sub>α</sub> of P-Y574 was pulled in the direction of R614, so that a wide gap was maintained between T546-C<sub>α</sub> and P-Y574-C<sub>α</sub>, fluctuating with an average width of 8.7 Å (Figure 7B). In the case of Y574F, its C<sub>α</sub> hardly moved in the

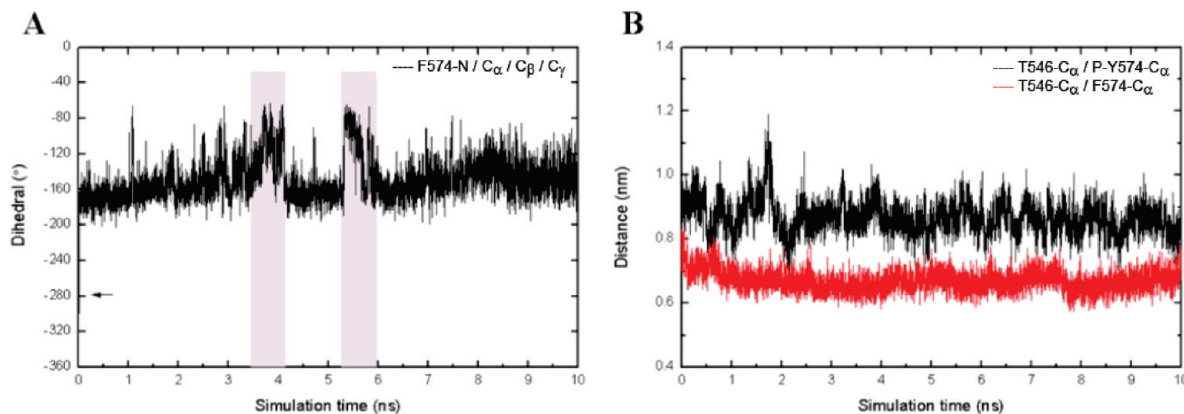


FIGURE 7: Simulation of the Y574F system. (A) Dihedral angle of F574-N/C<sub>α</sub>/C<sub>β</sub>/C<sub>γ</sub>, with two brief flipping events highlighted. (B) Time-dependent variation of the distance between T546-C<sub>α</sub> and P-Y574-C<sub>α</sub> in the P-Y574 system (black) and the distance between T546-C<sub>α</sub> and F574-C<sub>α</sub> in the Y574F mutant system (red).

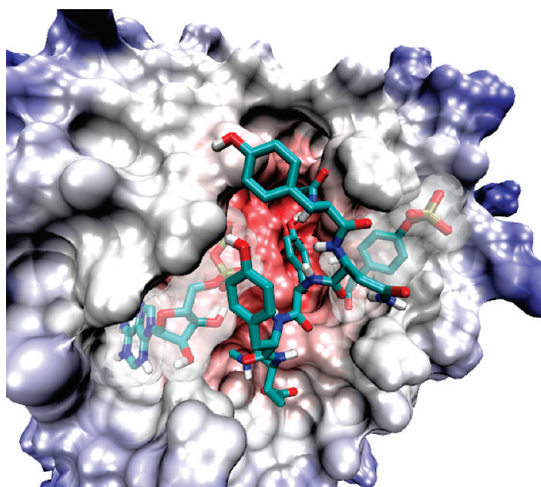


FIGURE 8: Docking of the C-terminal Tyr cluster peptide YNYYG into the activated (flipped P-Y574) Etk active site. The red, white, and blue colors represent the inner, middle, and outer region of the protein, respectively.

same direction and the distance between T546-C<sub>α</sub> and F574-C<sub>α</sub> remained ~2 Å shorter than that between T546-C<sub>α</sub> and P-Y574-C<sub>α</sub>. As a result, the narrow spacing in the active site would hinder the access of the substrate to the active site.

**Docking the C-Terminal Tyrosine Cluster into the Active Site.** To verify whether the conformational change of the P-Y574 side chain would be sufficient to allow for the entry of the tyrosine substrate to the active site and interact with catalytic residues, we synthesized the C-terminal Tyr cluster peptide (YSYGYN-YYGYSYSEKE). Unfortunately, this peptide was insoluble, likely because of multiple tyrosines, which are prone to aggregation. We therefore docked this peptide into the active site of the P-Y574 model, resulting from the 10 ns MD simulation using AutoDock (version 4.02) (29). Because the tyrosine cluster peptide is quite long, we selected three segments consisting of five residues from the tyrosine cluster (YNYYG, YGYSY, and YYGYS). These peptides were manually capped with an acetyl group on the C terminus and methylamine on the N terminus. Figure 8 shows the docking of YNYYG into the Etk active site. Because the side chain of P-Y574 has rotated away, the tyrosine cluster was readily accommodated in the active site. The tyrosine residue in the center of the peptide was able to approach the Etk catalytic center for phosphorylation. The combined free energy from docking was -10.43 kcal/mol. Docking of YGYSY and

Table 1: SASA of Side Chains of the Catalytic D567, D569, and D647 in Both P-Y574 and Y574F Mutant

SASA (nm <sup>2</sup> )	wild type (P-Y574)	Y574F mutant
ASP567	0.0890	0.0603
ASP569	0.320	0.198
ASP647	0.178	0.109

YYGYS also gave rise to similar results, further confirming that Y574 flipping is necessary and sufficient for the catalytic activity of Etk.

**Influence on Walker-A' and Walker-B Aspartic Residues by the P-Y574 Switch.** The aspartic acid residues D567, D569 (Walker-A' motif), D647 (Walker-B motif) are known to participate in the catalytic process. All three residues are found within or close to the  $\beta$  sheets, maintaining their positions for proper function. During the simulation, no significant conformational change was observed on the short side chains of these three aspartic residues, further supporting the notion that, during Etk activation, only the P-Y574 side chain experiences significant positional change and the active site remains unchanged. We calculated the solvent-accessible surface area (SASA) of side chains of the catalytic aspartic acids using a 1.4 Å solvent radius, following the 10 ns simulation of both the wild-type and Y574F Etk (Table 1). The SASA of the Y574F mutant is ~40% lower than that of the wild type. This difference is clearly due to the blockage of the active site by the Y574F side chain, reducing the contact area of the catalytic aspartic acid residues with the solvent.

**Binding of Cofactor ATP to Etk.** The activity of Etk depends upon not only the switch of P-Y574-R614 but also binding of ATP to the active site with an appropriate orientation. We previously determined that the binding constant  $K_M$  of ATP for Etk is ~5 mM, while the R572A mutant exhibited slightly lower  $K_M$  and the Y574F exhibited slightly higher  $K_M$  (results not published).

The mutational study of K540M on Wzc (equivalent of Etk K545M) suggested that the electrostatic interaction between positive-charged Lys and phosphate group(s) is the key for recruiting ATP (14). In the crystal structure of Etk, residue K545 lies in close vicinity to  $\beta$ -phosphate of ADP (11). The docking position of ADP in the Etk active site that we obtained is completely consistent with that from the crystal structure (11). The binding energy of ADP is calculated as -8.4 kcal/mol.

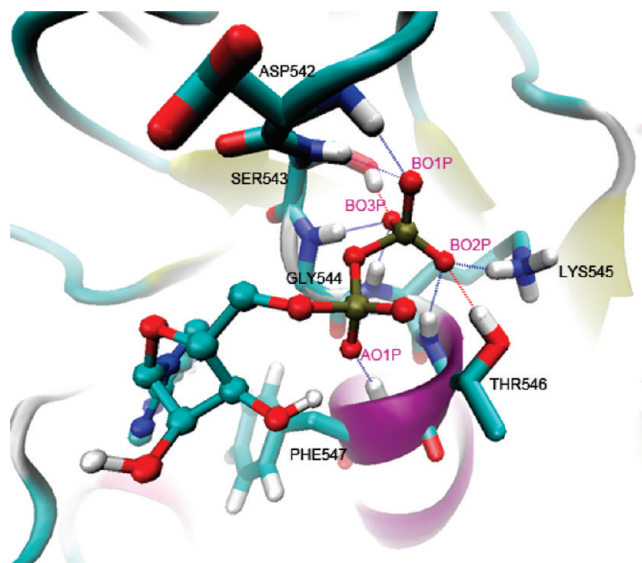


FIGURE 9: Schematic diagram of hydrogen bonds between ADP phosphate groups and residues 542–547. Blue and red colors represent nitrogen and oxygen atoms.

Table 2: Occupancy of Hydrogen Bonds between Etk and ADP Phosphates during the 10 ns MD Simulation

on Etk	on ADP $\beta$ -phosphate		
	O <sub>1</sub> (%)	O <sub>2</sub> (%)	O <sub>3</sub> (%)
Asp542-N	19.96	0.52	0.37
Ser543-N	26.57	0.77	32.43
Ser543-O <sub>γ</sub>	0.03	1.80	94.88
Gly544-N	39.71	0.57	21.06
Lys545-N <sub>ζ</sub>	0.09	10.65	10.13
Lys545-N	0.00	1.40	58.52
Thr546-O <sub>γ</sub> <sup>1</sup>	0.00	15.54	0.00
Thr546-N	0.02	17.62	0.00

During the 10 ns simulation, although the conformation of adenosine changed slightly, the  $\alpha$ - and  $\beta$ -phosphate groups remained in their original positions. The electrostatic interaction was not the only force that maintained the position of ADP. The  $\alpha$ - and  $\beta$ -phosphate groups of ADP were surrounded by residues 542–547 of Etk. All of the peptide NH groups were oriented toward ADP and formed hydrogen bonds with the phosphate groups. In addition, S543 and T546 also formed hydrogen bonds with ADP through their side-chain hydroxyl groups (Figure 9).

We calculated the occupancy of hydrogen bonds between Etk and ADP phosphate groups in the simulation. With the maximal angle of 30° and the longest distance of 3.5 Å as criteria for hydrogen bonding, we observed high occupancy of the hydrogen bonds between the ADP  $\beta$ -phosphate group and its surrounding residues (Table 2). The ADP  $\alpha$ -phosphate group also formed hydrogen bonds with the amide groups of T546 and F547. These hydrogen bonds not only help orient the cofactor to be suitable for phosphorylation but also assist K545 to interact with the cofactor via electrostatic interaction.

## CONCLUSION

Bacterial protein tyrosine kinases were largely an untapped territory until the past decade. While the first structure of a bacterial protein kinase (*E. coli* tyrosine kinase Etk) was

published recently, the proposed activation mechanism involving the side-chain flipping of P-Y574 to interact with R614 lacked direct support from crystallographic data (11). On the basis of MD simulation, our results confirmed that the active site is unblocked by the flipping of the phosphorylated Y574 side chain. The flipping of P-Y574 took place very early (at 460 ps) during our 10 ns simulation. This protein tyrosine kinase activation represented by *E. coli* Etk is likely applied to Gram-negative bacterial homologues that possess the conserved Y574- and R614-equivalent residues.

The electrostatic interaction between phosphorylated Y574 and R614 is a critical factor driving P-Y574 flipping. In the MD simulation, we found that R572, a conserved residue in Gram-negative bacteria, appears to exhibit a regulatory role through its interaction with P-Y574 during conformational change. The R572A mutation and its biochemical analysis provide experimental support for the previously unidentified regulatory role of R572. In addition, the simulation of the Y574F mutant explains the kinase activity, albeit low, because the side chain did flip out occasionally to render residual kinase activity. Using the flipped P-Y574 end-of-simulation model, we were able to dock a partial Etk C-terminal Tyr cluster into the opened active site. The docking position of ADP completely agrees with the crystal structure and shows that the  $\beta$ -phosphate forms multiple hydrogen bonds with Etk active-site residues. These interactions maintain the orientation of ATP during catalysis.

## SUPPORTING INFORMATION AVAILABLE

MD trajectory of the flipping of P-Y574 of Etk in the first 1 ns of the simulation. This material is available free of charge via the Internet at <http://pubs.acs.org>.

## REFERENCES

- Roberts, I. S. (1996) The biochemistry and genetics of capsular polysaccharide production in bacteria. *Annu. Rev. Microbiol.* 50, 285–315.
- Whitfield, C., and Paiment, A. (2003) Biosynthesis and assembly of Group 1 capsular polysaccharides in *Escherichia coli* and related extracellular polysaccharides in other bacteria. *Carbohydr. Res.* 338, 2491–2502.
- Dong, C., Beis, K., Nesper, J., Brunkan-Lamontagne, A. L., Clarke, B. R., Whitfield, C., and Naismith, J. H. (2006) Wza the translocon for *E. coli* capsular polysaccharides defines a new class of membrane protein. *Nature* 444, 226–229.
- Whitfield, C. (2006) Biosynthesis and assembly of capsular polysaccharides in *Escherichia coli*. *Annu. Rev. Biochem.* 75, 39–68.
- Doublet, P., Grangeasse, C., Obadia, B., Vaganay, E., and Cozzone, A. J. (2002) Structural organization of the protein-tyrosine autokinase Wzc within *Escherichia coli* cells. *J. Biol. Chem.* 277, 37339–37348.
- Collins, R. F., Beis, K., Dong, C., Bottig, C. H., McDonnell, C., Ford, R. C., Clarke, B. R., Whitfield, C., and Naismith, J. H. (2007) The 3D structure of a periplasm-spanning platform required for assembly of Group 1 capsular polysaccharides in *Escherichia coli*. *Proc. Natl. Acad. Sci. U.S.A.* 104, 2390–2395.
- Nesper, J., Hill, C. M., Paiment, A., Harauz, G., Beis, K., Naismith, J. H., and Whitfield, C. (2003) Translocation of group 1 capsular polysaccharide in *Escherichia coli* serotype K30. Structural and functional analysis of the outer membrane lipoprotein Wza. *J. Biol. Chem.* 278, 49763–49772.
- Reid, A. N., and Whitfield, C. (2005) Functional analysis of conserved gene products involved in assembly of *Escherichia coli* capsules and exopolysaccharides: Evidence for molecular recognition between Wza and Wzc for colanic acid biosynthesis. *J. Bacteriol.* 187, 5470–5481.
- Ilan, O., Bloch, Y., Frankel, G., Ullrich, H., Geider, K., and Rosenshine, I. (1999) Protein tyrosine kinases in bacterial pathogens are associated with virulence and production of exopolysaccharide. *EMBO J.* 18, 3241–3248.
- Vincent, C., Doublet, P., Grangeasse, C., Vaganay, E., Cozzone, A. J., and Duclos, B. (1999) Cells of *Escherichia coli* contain a protein-tyrosine

- kinase, Wzc, and a phosphotyrosine-protein phosphatase, Wzb. *J. Bacteriol.* 181, 3472–3477.
11. Lee, D. C., Zheng, J., She, Y. M., and Jia, Z. (2008) Structure of *Escherichia coli* tyrosine kinase Etk reveals a novel activation mechanism. *EMBO J.* 27, 1758–1766.
  12. Paiment, A., Hocking, J., and Whitfield, C. (2002) Impact of phosphorylation of specific residues in the tyrosine autokinase, Wzc, on its activity in assembly of Group I capsules in *Escherichia coli*. *J. Bacteriol.* 184, 6437–6447.
  13. Grangeasse, C., Cozzzone, A. J., Deutscher, J., and Mijakovic, I. (2007) Tyrosine phosphorylation: An emerging regulatory device of bacterial physiology. *Trends Biochem. Sci.* 32, 86–94.
  14. Grangeasse, C., Doublet, P., and Cozzzone, A. J. (2002) Tyrosine phosphorylation of protein kinase Wzc from *Escherichia coli* K12 occurs through a two-step process. *J. Biol. Chem.* 277, 7127–7135.
  15. Cowan-Jacob, S. W. (2006) Structural biology of protein tyrosine kinases. *Cell. Mol. Life Sci.* 63, 2608–2625.
  16. Lindahl, E., Hess, B., and van der Spoel, D. (2001) GROMACS 3.0: A package for molecular simulation and trajectory analysis. *J. Mol. Model.* 7, 306–317.
  17. Hansson, T., Nordlund, P., and Aqvist, J. (1997) Energetics of nucleophile activation in a protein tyrosine phosphatase. *J. Mol. Biol.* 265, 118–127.
  18. Berendsen, H. J. C., Grigera, J. R., and Straatsma, P. (1987) The missing term in effective pair potentials. *J. Phys. Chem.* 91, 6269–6271.
  19. Berendsen, H. J. C., Postma, J. P. M., van Gunsteren, W. F., DiNola, A., and Haak, J. R. (1984) Molecular dynamics with coupling to an external bath. *J. Chem. Phys.* 81, 3684–3690.
  20. Darden, T., York, D., and Pedersen, L. (1993) Particle mesh Ewald: An  $N \log(N)$  method for Ewald sums in large systems. *J. Chem. Phys.* 98, 10089–10092.
  21. Frisch, M. J., Trucks, G. W., Schlegel, H. B., Scuseria, G. E., Robb, M. A., Cheeseman, J. R., Montgomery, J. A., Jr., Vreven, T., Kudin, K. N., Burant, J. C., Millam, J. M., Iyengar, S. S., Tomasi, J., Barone, V., Mennucci, B., Cossi, M., Scalmani, G., Rega, N., Petersson, G. A., Nakatsuji, H., Hada, M., Ehara, M., Toyota, K., Fukuda, R., Hasegawa, J., Ishida, M., Nakajima, T., Honda, Y., Kitao, O., Nakai,
  - H., Klene, M., Li, X., Knox, J. E., Hratchian, H. P., Cross, J. B., Bakken, V., Adamo, C., Jaramillo, J., Gomperts, R., Stratmann, R. E., Yazyev, O., Austin, A. J., Cammi, R., Pomelli, C., Ochterski, J. W., Ayala, P. Y., Morokuma, K., Voth, G. A., Salvador, P., Dannenberg, J. J., Zakrzewski, V. G., Dapprich, S., Daniels, A. D., Strain, M. C., Farkas, O., Malick, D. K., Rabuck, A. D., Raghavachari, K., Foresman, J. B., Ortiz, J. V., Cui, Q., Baboul, A. G., Clifford, S., Cioslowski, J., Stefanov, B. B., Liu, G., Liashenko, A., Piskorz, P., Komaromi, I., Martin, R. L., Fox, D. J., Keith, T., Al-Laham, M. A., Peng, C. Y., Nanayakkara, A., Challacombe, M., Gill, P. M. W., Johnson, B., Chen, W., Wong, M. W., Gonzalez, C., Pople, J. A. (2004) Gaussian 03, Revision C.02, Gaussian, Inc., Wallingford, CT.
  22. Lee, C., Yang, W., and Parr, R. G. (1988) Development of the Colle–Salvetti correlation-energy formula into a functional of the electron density. *Phys. Rev. B: Condens. Matter Mater. Phys.* 37, 785–789.
  23. Rassolov, V. A., Pople, J. A., Ratner, M. A., and Windus, T. L. (1998) 6-31G\* basis set for atoms K through Zn. *J. Chem. Phys.* 109, 1223–1229.
  24. Hariharan, P. C., and Pople, J. A. (1973) Theoretical chemistry accounts: Theory, computation, and modeling. *Theor. Chim. Acta* 28, 213–222.
  25. Gordon, M. S., Binkley, J. S., Pople, J. A., Pietro, W. J., and Hehre, W. J. (1982) Self-consistent molecular-orbital methods. 22. Small split-valence basis sets for second-row elements. *J. Am. Chem. Soc.* 104, 2797–2803.
  26. Binkley, J. S., Pople, J. A., and Hehre, W. J. (1980) Self-consistent molecular orbital methods. 21. Small split-valence basis sets for first-row elements. *J. Am. Chem. Soc.* 102, 939–947.
  27. Wlodek, S. T., Clark, T. W., Scott, L. R., and McCammon, J. A. (1997) Molecular dynamics of acetylcholinesterase dimer complexed with tacrine. *J. Am. Chem. Soc.* 119, 9513–9522.
  28. Humphrey, W., Dalke, A., and Schulten, K. (1996) VMD: Visual molecular dynamics. *J. Mol. Graphics* 14, 33–38.
  29. Morris, G. M., Goodsell, D. S., Halliday, R. S., Huey, R., Hart, W. E., Belew, R. K., and Olson, A. J. (1998) Automated docking using a Lamarckian genetic algorithm and an empirical binding free energy function. *J. Comput. Chem.* 19, 1639–1662.